

Anchor Calibration for Real-Time-Measurement Localization Systems

Peter Krapež and Marko Munih¹, *Member, IEEE*

Abstract—This article investigates the effect of additional calibration modules (CMs) in a 3-D real-time localization system during the calibration of the anchor position. A quick calibration is desirable for new anchors that are positionally undetermined in the working coordinate system. Three localization methods were tested for the anchor calibration: multidimensional scaling, semidefinite programming, and iterative trilateration. First, the accuracy of the anchor localization was studied by simulating a change in the number of additional CMs and their positions. Second, tests on a real system with ultrawideband modules were performed to validate the improvements in the anchor calibration when using the additional CMs. The experimental results revealed an improvement in the anchor localization for all three methods, where the average positional error was improved by 0.01 m in the first scenario and 0.30 m in the second scenario. The MDS method had the best absolute performance, with an average positional error that was as much as two times less in comparison with the other two methods. This investigation demonstrates that the positional error can be successfully reduced by using additional CMs. The calibration of anchor positions in the working coordinate system using additional CMs resulted in a 3-D error of less than 0.32 m.

Index Terms—3-D anchor localization, anchor calibration, calibration modules (CMs), position measurement, time-of-flight (ToF), ultrawideband (UWB) technology.

I. INTRODUCTION

AUTONOMOUS mobile applications used in everyday life and the localization demands of the Internet of Things are increasing. These include automatic lawnmowers, drones [1], AGVs, smart sensors [2], and even automated forklifts that leave the production site's doors to load a truck. Real-time localization based on radio trilateration (TRI) requires a number of radio anchors. To extend the range, new anchors are needed, together with the calibration of the anchor position in space. Even changes in the working site may require anchor repositioning and, consequently, a new anchor calibration. This is the advantage of localization systems with automatic anchor calibration.

Manuscript received March 9, 2020; accepted June 11, 2020. Date of publication June 29, 2020; date of current version November 10, 2020. This work was supported in part by the Slovenian Research Agency through the Research Core Funding under Grant P2-0228 and the Young Researcher Founding, and in part by the European Commission through the CYBERLEGS Plus Project under Grant 731931, within the H2020 Framework (H2020-ICT-25-2016-2017). The Associate Editor coordinating the review process was Dr. Daniele Fontanelli. (Corresponding author: Peter Krapež.)

The authors are with Laboratory of Robotics, Faculty of Electrical Engineering, University of Ljubljana, SI-1000 Ljubljana, Slovenia (e-mail: peter.krapez@fe.uni-lj.si; marko.munih@robo.fe.uni-lj.si).

Color versions of one or more of the figures in this article are available online at <https://ieeexplore.ieee.org>.

Digital Object Identifier 10.1109/TIM.2020.3005258

In real-time localization systems (RTLs), the mobile unit is localized by measuring the distances to static modules, i.e., anchors, with a known position. The positions of the anchors can be determined in two ways. The first option is to measure the anchor position with a measuring system, such as a tachymeter, utilizing geodetic procedures. An alternative is to calibrate the anchor position by measuring intermodule distances and computing the locations with mathematical algorithms. Although the use of external measurement equipment provides anchor positions with high accuracy, the anchors have to be constructed and placed in such a way that enables an external measurement, which means that the ability to reconfigure is reduced. The second anchor-calibration approach represents an effortless method for anchor localization and could contribute to RTLs as a turnkey product where the end user can do the entire setup of the RTL without additional equipment.

Numerous indoor RTLs are presented in literature and are available as products [3]. He and Dong [4] presented RTL based on ultrawideband (UWB) technology for the asynchronous time difference of arrival localization. Kolakowski [5] developed a hybrid system where UWB is used for the first-time calibration of Bluetooth Low Energy RTLs. Wang *et al.* [6] used UWB as a secondary system for frequent calibration of primary RTLs based on the *K*-band Doppler radar sided with a gyroscope. Martinelli *et al.* [7] and Wang *et al.* [8] presented localization in a harsh industrial environment. All the abovementioned RTLs use anchors system, with known positions, for localizing mobile modules.

A lot of work was carried out in another domain, i.e., mobile sensor localization without the use of anchor modules. The problem is the same as a stationary anchor calibration because, in both cases, no anchor modules with known positions are present. The localization of new modules can be conducted with a global approach. In this case, the positions of the old and new modules are calculated simultaneously and updated for the old and new modules. An alternative to that is the iterative approach, where only the positions of the new modules are defined.

Previous work relied on multidimensional scaling (MDS) [9], [10] as one of the global approaches to module localization. Shang *et al.* [11] presented a method that uses only the connectivity information between the modules. The authors implemented different approaches to constructing and refining the Euclidian distance matrix (EDM), where all the approaches share a common course of first acquiring the EDM and then using the MDS to compute the relative module

coordinates. Optionally, if more than three module positions are known, the relative module coordinates can be transformed to the global coordinate system. Another global approach is to use semidefinite programming (SDP), shown in [12] and [13], while, in [13], the EDM completion problem is addressed.

An iterative localization algorithm called sweep is explained in [14], where the iterative TRI is replaced by bilateration, so more modules can be localized. In this way, two possible locations for each new module are computed. All the possible locations are then included in the localization of the next modules, which results in a rapidly expanding number of solutions. The authors show how to reduce the number of possible module solutions by eliminating least-suitable ones. Priyantha *et al.* [15] presented a distributed localization algorithm for a network of sensors with the use of mass-spring optimization. Another distributed algorithm is shown in [16], where newly computed module coordinates are added to a set of already-localized modules.

Localization algorithms were used in the past for anchor calibrations in RTLSs. Kuang *et al.* [17] solved the localization problem by factorizing a compaction matrix, which contains information about the distances between anchor modules. The minimal noniterative solvers for the second and third space dimensions were explored. Here, the numbers of transmitting and receiving anchors are defined for each solver. Batstone *et al.* [18] used factorization of a compaction matrix, adopting the rank constraints of the compaction matrix for outlier detection. They are focused on problems with missing distances and outliers in real-time anchor calibration. The authors approached this problem by solving smaller graph problems and aligning their coordinate systems to create a global solution. The transformation was computed from the overlapping areas of smaller graphs.

Zhou *et al.* [19] presented an anchor calibration for the rotational time-difference-of-arrival and the MDS algorithm. The authors showed that MDS's accuracy rapidly increases when the number of anchors increases to ten. The algorithm for the anchor calibration presented in [20] computes more solutions with a solver using multidimensional, nonlinear least-squares fitting. Based on three fitness functions, the final solution is selected from different initial positions.

The application of an anchor calibration using a sweep algorithm was made by Nakamura and Sakamura [21]. By applying fully connected quadrilaterals from [22], the anchors were uniquely localized. The authors used TRI for the anchor calibration from three selected anchors, which defines the coordinate system. Using a method called robust quad check, no flip and flex ambiguities were ensured, which, in turn, improved the TRI algorithm.

Müller *et al.* [23] and Van de Velde *et al.* [24] introduced a new feature in the process of anchor calibration. An additional anchor (a new calibration module (CM) or temporary anchor) is used just for the purposes of anchor calibration. Müller *et al.* [23] presented an anchor-calibration method that uses bilateration. First, the seed anchors were computed; then, all of the other anchors were sorted in bilateration ordering, and their positions were computed with bilateration. For each

configuration, the stress is computed, and the best configuration is selected for the end result. The authors implemented a temporary anchor, which was placed in the system in a way that ranging using all of the anchors was possible. After the anchor calibration is completed, a temporary anchor is removed from the anchor system. With the temporary anchor placement, new measurements are added to the collection of intermodule distances so that the anchors without line-of-sight (LOS) can be localized.

Van de Velde *et al.* [24] introduced a technique similar to the simultaneous localization and mapping (SLAM) method. Rather than using sensors to scan the surroundings, it uses radio communications for the ranging between anchors. They used a calibration unit (CU) that was moved in space by the operator in order to collect the distance measurements between the anchors and the CU. When the CU is moved in a straight line, all the intermodule distances between the anchors can be computed, and by means of weighted least squares, the anchors' coordinates can be determined.

As outlined earlier, previous studies looked at different methods of anchor calibration, with most of the research focused on 2-D localization problems. This article investigates the problem of anchor localization in 3-D space by placing localized anchors in a working coordinate system. The possibility to decrease the anchors' localization error was explored through the use of an additional CU that contains CMs with known relative positions with respect to each other. In this research, the methods MDS and SDP [13] and an algorithm based on TRI [14], [20], [23] were compared. A series of simulations was executed first to evaluate the impact that the CU has on the anchor-localization error. Then, experiments on a real system for two scenarios with LOS and non-LOS (NLOS) conditions were performed to validate the simulation results. The anchor calibration implemented four CMs on the CU to provide several possibilities for the proposed calibration method. The final goal of this work was to evaluate and present an anchor-calibration method for improved anchor localization in an arbitrary coordinate system. To the best of our knowledge, this is the first attempt to examine the effect of implementing a new CU in an anchor calibration in terms of an anchor-localization error. The anchor was localized in a specific coordinate system, and, most importantly, in 3-D, not only a planar system.

II. ANCHOR-CALIBRATION METHOD WITH A CALIBRATION UNIT

To operate an RTLS, the positions of the anchors in a common working coordinate system must be known. Anchor calibration is a process of determining the anchors' relative positions from the measured distances between all the anchors and transforming them into a global (working) coordinate system. From N anchor modules, $M = \binom{N}{2}$ intermodule distances are measured, which are part of an EDM with a size of $N \times N$. The anchors' positions are obtained by minimizing the error

$$e_{ij} = \|a_i - a_j\| - d_{ij} \quad (1)$$

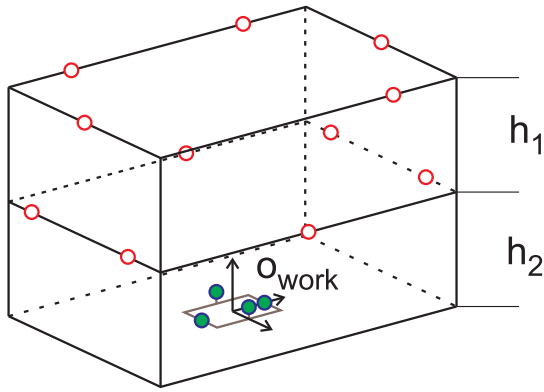


Fig. 1. Anchor calibration with CU.

where a_i and a_j are the positions of the anchors, and d_{ij} is the measured distance between the i th and the j th anchor.

The final positional error of the mobile unit in the RTLS is a superposition of not only the distance measurement error between the anchors and the mobile unit but also the positional error arising from the placement of the anchors used in the RTLS. Therefore, decreasing the anchor’s positional error and improving the anchor’s position in a working coordinate system based on an anchor calibration are the motivation for this work.

When designing the RTLS, the best conditions, within the environmental constraints in which it will operate, are desired for radio communications between the anchors and the mobile unit modules. Such conditions are usually ensured by placing the anchors at elevated positions (see Fig. 1) so that the radio signal is not obstructed by people moving around and other obstacles. With the aforementioned anchor configuration, the modules are not deployed through the full possible height range of the RTLS setup. Therefore, a setup that includes the CU and places it on the floor has been adopted. In this way, the entire range of distances in the z -axis is covered (green dots in Fig. 1), and the full spatial information about the space in which the RTLS operates is ensured. The idea of the CU is introduced in [23] and [24], but the purpose of the CU in this article is different. Here, the CU is implemented and tested as a calibration method for initializing the new RTLS setup and localizing the new anchors in a defined working coordinate system (see Fig. 1), where no prior information about the anchors’ positions is available. With the CU placed correctly, the minimum positional error of the anchors is achieved. The CU in our case is placed in such a way that the relation to the working coordinate system is known. The computed positions of the anchors are then aligned with the CU, so placing them in the working coordinate system.

In this article, the anchor-calibration method in 3-D is validated. It can be used for localizing the anchors in an arbitrary working coordinate system with additional CMs. The method can be adopted for scenarios where not all the anchors are in each others radio ranges. Smaller anchor configurations are localized independently of each other, and afterward, an alignment with the common anchors is performed.

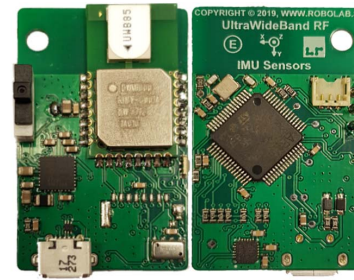


Fig. 2. Top and bottom sides of the designed board with the UWB radio module.

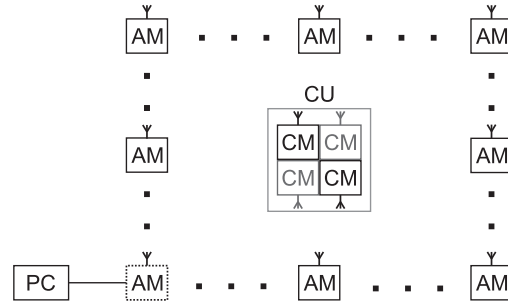


Fig. 3. System configuration block diagram.

III. SYSTEM DESCRIPTION

A. UWB Modules

The test system consists of 18 printed circuit boards with UWB DWM1000 modules, an STM32L4 microprocessor, and a USB port (see Fig. 2). The modules are enclosed in a protective plastic housing and can be placed in any position with a customized attachment plate.

After all the anchors are placed in the desired configuration, the master anchor is connected to the PC via the USB (see Fig. 3). All the incoming and outgoing data from the PC to the anchors and vice versa are relayed through the master anchor.

B. Distance Measurements

The distances between the modules were computed using the time-of-flight (ToF) method for the radio signal traveling between two modules. For the ToF calculation, a two-way-ranging equation was used [25]. After the modules’ deployment, all the intermodule distances were measured,

Algorithm 1 Distance Measurements of One Set

Initialization list = all anchor and CU addresses

for all addresses in list **do**

for all addresses in list **do**

 gather 250 distance measurements

 send measurements to master anchor

 send measurements to PC

end for

end for

Finalization build EDM from distance measurements

as described in Algorithm 1. For the experiment, the decision was made to have 40 measurement sets for system and calibration method stability analysis. The measurements were then filtered for any outliers and passed to the localization algorithms for processing. The outlier filtering involved applying a threshold for the Mahalanobis distance for each sample. The filtered values were replaced with a mean value before the filtration, so the number of samples remained the same after the filtering [26].

C. UWB Module Calibration

Calibration was made for each pair of anchors and CM in the same experimental environment. The calibration measurements were taken from 1 to 32 m in 1-m increments. Several regressions were made on the measured data. Since all the modules had similar error characteristics, a higher order of polynomial regression was used. The best fit was with the sixth order of polynomial regression. An average RMSE of 0.03 m was obtained for all 180 calibration regressions. The average distance error over all the distance measurements and all the measurement sets after the calibration was 0.07 m. Guo *et al.* [1] suggested the calibration of the UWB modules with linear regression for two intervals with the ranges 0–1.5 and 1.5–8 m. Due to the decreasing accuracy of the measurements to 1.5 m, we used the same sixth-order polynomial regression for the entire calibration distance.

IV. METHODOLOGY

A. Performance Metrics

Two performance metrics are presented. The first metric is determining the quality of fit between the localization and the measured data sets. The second metric is used to evaluate the error between the calculated and the reference coordinates.

The mean-square-error distance or stress can be defined as

$$\text{Stress} = \sqrt{\frac{\sum_{i=1}^M (\hat{d}_i - d_i)^2}{d_i}} \quad (2)$$

where M is the number of intermodule distances for N modules, \hat{d}_i is the distance calculated from the localization algorithms, and d_i is the measured distance or the distance from the simulation. Stress is used in the algorithm as an internal performance metric in the TRI localization method.

The average-position error (APE) [22] or mean-square-position error can be written as

$$\text{APE} = \frac{\sum_{i=1}^N \sqrt{(\hat{\mathbf{a}}_i - \mathbf{a}_i)(\hat{\mathbf{a}}_i - \mathbf{a}_i)^T}}{N} \quad (3)$$

where $\hat{\mathbf{a}}_i$ is the i th localized module, \mathbf{a}_i is its true position, and N is the number of modules.

For a comparison of errors, based on the individual coordinates, five combinations of coordinates as inputs for the APE computation were used: xyz (3-D), xy (2-D), x , y , and z coordinates. The notations of the APE for each coordinate combination are $\text{APE}(xy)$, $\text{APE}(x)$, $\text{APE}(y)$, and $\text{APE}(z)$, where the input argument presents the coordinates used for the APE computation. The APE without any input argument is used for the xyz combination.

For computing the APE, a rigid transformation has to be made to align the computing coordinates with the reference coordinates. The alignment is made with the least-square rigid-transformation method, as described in [27]. The same method was used to align the localized CU from the measurements with a known position of the CU.

B. Localization Methods

The aim of this article was to analyze the impact of using the CU on the APE in 3-D. To eliminate the effects of an incomplete Euclidean distance matrix (EDM) on the anchor-calibration accuracy, localization methods that use the complete EDM were used. A full EDM was constructed with measurements of all the intermodule distances. The only exceptions were the distances between the CM on the CU, which were computed from their known relative positions. One of the solutions for completing the EDM is described in [13] and another approach in [28], where smaller networks are joined if they have common modules in both subnetworks. We have used three localization algorithms: MDS [11], SDP [13], and TRI [14].

1) *Multidimensional Scaling*: MDS is a mathematical method for reducing the dimensions of multidimensional data. For the localization, the data are usually reduced to two or three dimensions, depending on whether we are localizing in 2-D or 3-D space. MDS reduces the EDM to lower-dimensional data (coordinates) in such a way that the distances between the computed points represent the input EDM.

For the MDS localization algorithm, the steps described in [11] were used. Due to the anchor setup, there was no problem with computing the missing EDM entries as a first step of the localizing algorithm since a full EDM could be obtained with measurements. For the second step, an MDS function implemented in MATLAB was used. The third step was used for the APE computations, as the computed coordinates from the algorithm were aligned with the reference coordinates and for the actual anchor calibration method when the computed coordinates were aligned with the CU coordinates.

2) *Semidefinite Programming*: For the second localization algorithm, the SDP algorithm from [13] was used. It uses SDP, i.e., a convex optimization procedure that minimizes the linear function. The optimized function is subjected to a constraint such that the affine combination of symmetric matrices is positive semidefinite [29]. A general approach when using SDP for a localizing problem is using relaxation to solve

$$\min_{\mathbf{Y} \geq 0, \mathbf{Y} \in \Omega} \|\mathbf{W} \circ (\kappa(\mathbf{Y}) - \mathbf{D})\| \quad (4)$$

where $\mathbf{Y} \in \Omega$ are linear restrictions, \mathbf{Y} is the positive semidefinite matrix, \mathbf{D} is the EDM, \mathbf{W} is the weight matrix, and \circ is the Hadaman product [12].

3) *Trilateration*: The final method for anchor localization, TRI, is based on TRI. Principles similar to the ones introduced in [14] were implemented. The TRI method uses $\binom{N}{4}$ different combinations of four initial anchors' combinations, where N

is the number of anchors and CMs in the system. Each initial anchors' combination gives one anchor-calibration solution. The positions of the initial anchors are $\mathbf{a}_1 = [0, 0, 0]^T$, $\mathbf{a}_2 = [d_{12}, 0, 0]^T$, $\mathbf{a}_3 = [a_{3x}, a_{3y}, 0]^T$, and $\mathbf{a}_4 = [a_{4x}, a_{4y}, a_{4z}]^T$ with

$$a_{3x} = \frac{d_{12}^2 + d_{13}^2 - d_{23}^2}{2d_{12}}, \quad a_{3y} = \sqrt{d_{13}^2 - \frac{(d_{12}^2 + d_{13}^2 - d_{23}^2)^2}{4d_{12}^2}} \quad (5)$$

$$a_{4x} = \frac{d_{12}^2 + d_{14}^2 - d_{24}^2}{2d_{12}}, \quad a_{4z} = \sqrt{d_{14}^2 - (a_{4x}^2 + a_{4y}^2)}$$

$$a_{4y} = \frac{d_{12}(d_{13}^2 + d_{14}^2 - d_{34}^2) - a_{3x}(d_{12}^2 + d_{14}^2 - d_{24}^2)}{2d_{12} a_{3y}}. \quad (6)$$

This defines the coordinate system for a solution [30], where d_{12} , d_{13} , d_{14} , d_{23} , d_{24} , and d_{34} are the distances between all four initial anchors.

After the initial anchors are localized, TRI is used to localize all of the other anchors. Later, the number of initial anchors is reduced to shorten the computational time by discarding the coplanar combinations of the initial anchors. A threshold for coplanarity was determined so that the anchors on the same surface of the cuboid were eliminated. Also, additional initial anchor combinations were removed from any subsequent computation so as to achieve a reduction in the computation time of 60%, without losing the accuracy of the anchors' coordinates. When all the suitable solutions of the anchor coordinates are computed, solutions with a stress parameter greater than a defined threshold are discarded. The algorithm output is a single set of anchor coordinates, which is an average value of the remaining solutions.

C. Simulation and Experimental Scenario Layouts

To explore the anchor-calibration method with the CU, two scenario layouts were designed.

The first scenario (marked as GYM), presenting the LOS conditions with a symmetrical anchor placement, had 16 of a total of 18 modules placed on rectangular edges as anchors (see Fig. 4). The experiments took place in a gym, where the modules were placed at two alternating heights along the borders of a rectangular field measuring 28×20 m. All 16 anchors were fixed on a wooden housing so that they could be placed on top of telescopic stands.

The second scenario (marked as LAB) had an asymmetrical placement of 12 anchors and NLOS conditions for several anchors pairs. The experiments were performed in the Laboratory of Robotics, which has a floor plan with dimensions of 10×12 m (see Fig. 5) and is occupied by equipment and by people who are moving around. The anchors were placed at three different heights so that the largest height difference was achieved. All 12 anchors were fixed to the wall with custom-designed wall mounts. The LAB scenario represents more complicated, realistic conditions, where the RTLS designer is limited by the range of suitable positions for the anchors.

The anchor-placement dimensions of both scenarios are presented in Table I. The maximum positional differences

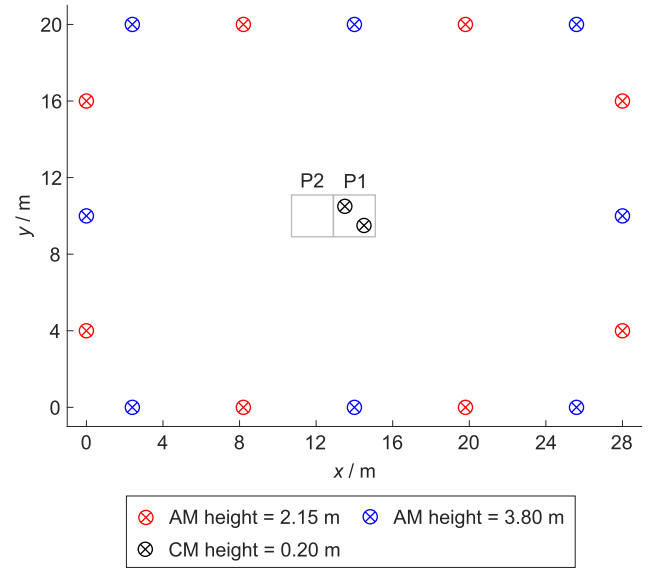


Fig. 4. Plane view of GYM scenario layout with 16 anchors and CU with two CMs in optimal (P1) and nonoptimal (P2) positions.

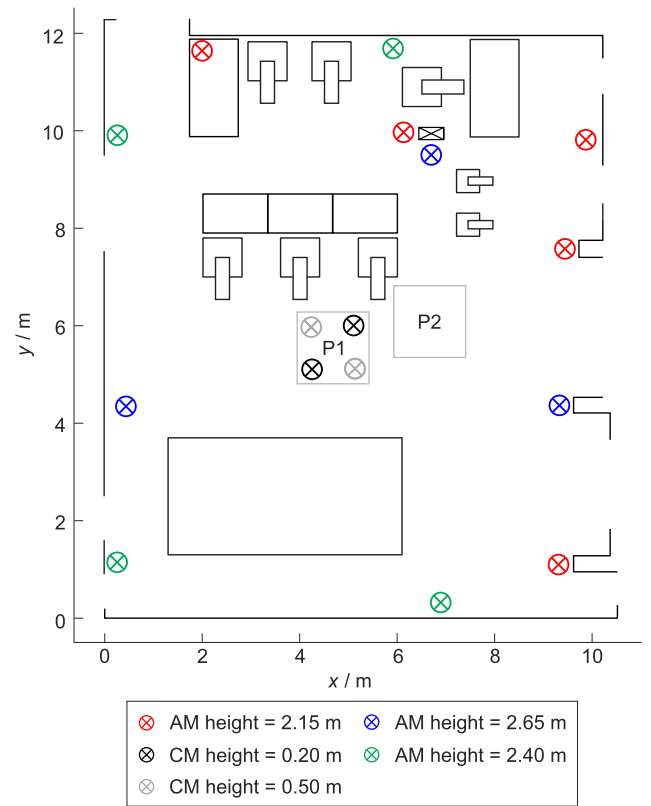


Fig. 5. Area with LAB scenario layout with 12 anchors and CU with two CMs in optimal (P1) and nonoptimal (P2) positions. The additional elements in the figure represent other objects in the laboratory.

TABLE I
ANCHORS' MAXIMUM POSITIONAL DIFFERENCES
FOR THE SCENARIOS GYM AND LAB

	GYM	LAB
Δx / m	28	10
Δy / m	20	12
Δz / m	1.45	0.50
CU Δz / m	3.40	2.45

between the anchors are presented in the first three rows, and the last row presents the height difference between the highest anchors and the CU.

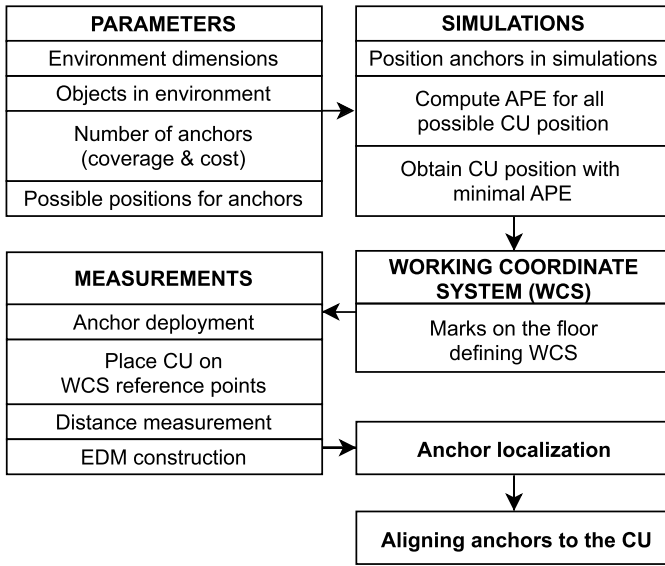


Fig. 6. Anchor calibration procedure flowchart.

D. Anchor Calibration

For the anchor calibration in the 3-D working coordinate system, at least four CMs on the CU are required. In the LAB scenario, additional two CMs were added to opposite corners on the CU (light-gray markers in Fig. 5). When the relationship between the CU and the working coordinate system is known, the alignment of the localized anchor with respect to the CU is possible.

The CU is a square plate with an edge length of 1 m. The CMs are placed on its corners, as shown in Fig. 5. The positions of the CMs are measured, and with that, the relative positions with respect to the edges and corners of the CU plate are known. That way, CMs' coordinates P_{CM} are defined in the CU's coordinate system: P_{CM}^{CU} . When CU is positioned on WCS' reference points, the transformation between coordinate systems T is known. With $P_{CU}^{WCS} = T P_{CU}$, CM coordinates can be transformed to WCS. The complete anchor-calibration procedure is presented in Fig. 6.

E. Ground Truth

Anchor-calibration method was evaluated experimentally with the measurement system. Ground-truth positions of the anchors were measured with a certified electronic tachymeter LeicaTPS 1201+, which represents the gold standard in reference-position measurements. The mounting plates for the anchors were designed in such a way that the reflective targets of the geodetic equipment could be fixed to them. After the geodetic measurements were made, the anchors were attached to the mounting plate with a known offset from the reflective target center (the measured reference point). To obtain the true reference coordinates, the offsets between the coordinate of the reflective target's center and the anchor's antenna were applied to the reflective target's coordinates. In the second measurement series, wall mounts were designed for the anchors. The CU reference positions were measured in the same coordinate system as the anchor reference positions. The reference coordinates of the reflective targets were computed with an uncertainty of less than 1 mm.

V. SIMULATIONS

Sections V-A and V-B describe the simulation configurations, parameters, and the corresponding results. The simulations were performed to evaluate the impact of the CU on the anchors' APE obtained using the three localization methods. The purpose of the simulations was to explore the different parameters of the CU before testing with the actual system. The conclusions drawn from the simulations were then used in the experiments.

A. Position of the Calibration Unit and the Number of Calibration Modules

The tested parameters were the number of CMs used and their positions. The notation for the different numbers of CMs is AX, where X is the number of CMs on the CU. All the configurations are presented in Fig. 7, where the crossed black circles represent one CM on a CU. Each gray square's side has a length of 1 m. Simulations were made for each CU configuration. In the simulations, the CU position (red cross in Fig. 7) changed in the x , y , and z coordinates of the GYM or LAB area (see Figs. 4 and 5), as described in Table II. To evaluate the impact of the CU on the anchor localization, a configuration without a CU, indicated as A0, was used. In the simulations, the noise was modeled with a Gaussian zero-mean random variable, which had a standard deviation (STD) of 0.15 m [24]. The same set of random seed numbers was used for all three localization methods in 100 simulation runs. For the APE calculation, only the positions of the anchors were used.

The results from 100 simulation runs were averaged so that a single APE value was obtained for each CU position. From all of the CU positions, the one with the smallest APE was chosen as the final result presented in Table III.

For the A1 configuration, the APE was 28% and 26% lower compared with the A0 configuration when using the MDS and the TRI methods in the GYM scenario. In the LAB scenario, the APE was 76% and 47% lower. When the maximum number of CMs was added (A16 configuration), the APE was lowered by 62% and 34% compared with the A0 configuration for the MDS and the TRI methods in the GYM scenario. In the LAB scenario, the APE was lowered by 87% and 65% when using the MDS and the TRI method. APE improvements for the selected A2 configuration are presented in the bottom row of Table III. Compared with the other two methods, the SDP method had significantly higher APE values in the A0 configurations. This method proved to be noise sensitive, especially in the A0 configuration. When using the CU with the SDP method, simulations had better results, and the trend of the decreasing APE with respect to the additional CMs can be seen in Table III, from the A1 configuration onward.

The biggest APE improvement per number of used CMs was seen when using the A1 configuration. The improvement with the MDS and TRI methods was 0.011 and 0.012 m/CM for the GYM scenario and 0.064 and 0.045 m/CM for the LAB scenario. For the A2 configuration, the APE improvement per CM was 50% smaller compared with the A1 configuration. The only exception was in the GYM scenario and with the

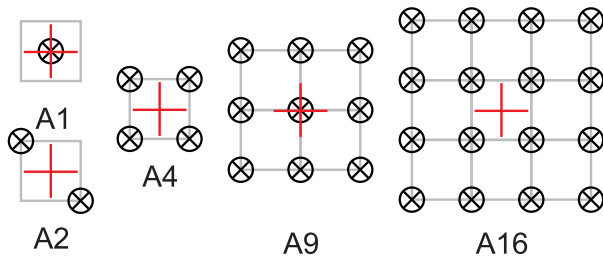


Fig. 7. Configuration of the CMs used in the simulations.

TABLE II
CU POSITION RANGES FOR THE SCENARIOS
GYM AND LAB IN SIMULATIONS

	GYM	LAB	
x / m	0–28.0	0–8.0	step 1.0 m
y / m	0–20.0	0–10.5	step 1.0 m
z / m	0–2.0	0–2.0	step 0.2 m

TABLE III

APE OBTAINED BY SIMULATIONS FOR THE A0, A1, A2, A4, A9, AND A16 SIMULATION CONFIGURATIONS FOR ALL THREE LOCALIZATION METHODS FOR THE SCENARIOS GYM AND LAB

	GYM			LAB		
	MDS	SDP	TRI	MDS	SDP	TRI
A0 / m	0.039	0.237	0.047	0.084	0.171	0.095
A1 / m	0.028	0.018	0.035	0.020	0.017	0.050
A2 / m	0.025	0.017	0.036	0.017	0.015	0.048
A4 / m	0.020	0.016	0.031	0.014	0.011	0.037
A9 / m	0.017	0.013	0.030	0.012	0.010	0.035
A16 / m	0.015	0.011	0.031	0.011	0.009	0.033
$\Delta A2$ / m	0.014	0.220	0.011	0.068	0.156	0.047

MDS method, where the APE was improved by 64%. For the A4 configuration, the improvements were less than 30%, for the A9 configuration, less than 15%, and for the A16 configuration, less than 10% of those seen in the A1 configuration.

The surf plot in Fig. 8 illustrates how the changes in the CU position affect the APE values for the A2 configuration and the TRI method. From all the positions verified in the simulations, the smallest APE value along the z coordinate was selected for this plot. All three localization methods had a similar spherical shape of error but different absolute values. The APE was the smallest when the CU was in the central position for the GYM scenario and outside of it for the LAB scenario. In the LAB scenario, localization methods had smaller deviations of the CU position for up to 0.5 m. The smallest APE values from simulations of the A2 configuration are presented in Table III. Optimal positions for both scenarios are presented in Figs. 4 and 5.

B. Height Difference Between the Anchors and the Calibration Unit

Simulations were used to evaluate how different height differences along the z coordinate between the anchors and the CU impact on the anchors' APE. Height-difference simulations used the x and y coordinates from the positions with the

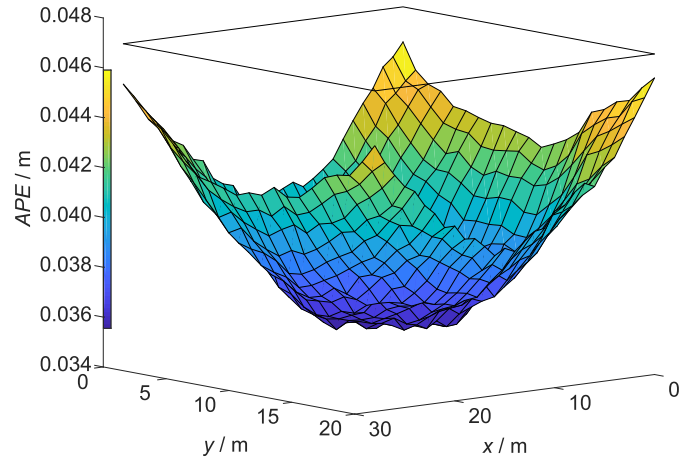


Fig. 8. A2 simulation results (surf plot) and a result of the A0 simulation (black square) for the TRI localization method. Values on the surf plot represent the smallest average APE along the z -axis. The presented values in the figure are average values computed from 100 simulation runs for each x , y , and z coordinates.

TABLE IV

APE OBTAINED BY A2 SIMULATIONS WHERE THE HEIGHT DIFFERENCE BETWEEN THE CU AND THE HIGHEST ANCHOR WAS INCREASED FOR THE OPTIMAL X AND Y POSITIONS

distances / m	3.6	5.0	10.0	15.0	20.0	28.0
GYM MDS / m	0.025	0.020	0.012	0.010	0.009	0.009
GYM SDP / m	0.017	0.014	0.010	0.008	0.008	0.007
GYM TRI / m	0.036	0.029	0.018	0.015	0.014	0.014
LAB distances / m	2.7	3.1	2.7	5.1	6.5	12.0
LAB MDS / m	0.015	0.014	0.012	0.011	0.010	0.009
LAB SDP / m	0.014	0.012	0.011	0.009	0.009	0.008
LAB TRI / m	0.048	0.029	0.016	0.013	0.012	0.015

smallest APE, acquired from previous simulations. The height difference was increased throughout the simulation, up to 28 m in the GYM scenario and 12 m in the LAB scenario. With these values, the height differences between the anchors and the CMs were the same as the longest edge of the anchor's floor layout (see Table I). These conditions provide better spatial information for the anchor calibration, as additional CMs improve the coplanarity of the anchor configuration.

The APE results of the simulations for six different heights are shown in Table IV. In the GYM scenario, the APE improvement was the greatest in the range of height differences up to 15.0 m. This is approximately half the length of the longest edge of the anchor's floor layout. For this height difference, the APE declined by 60% with the MDS, 53% with the SDP, and 58% with the TRI method compared with the APE in the A2 configuration from Table III.

In the LAB scenario, the APE improvement was the largest in the range of height differences up to 5.1 m, which is again approximately half the length of the longest edge of the anchor's floor layout. For the height difference of 5.1 m, the APE declined by 27% with the MDS, 36% with the SDP, and 67% with the TRI method compared with the APE in the A2 configuration from Table III.

TABLE V
EXPERIMENTAL APE FOR FIRST POSITION OF CU FOR ANCHOR
LOCALIZATION WHEN A0 AND A2 IS USED FOR BOTH SCENARIOS

	GYM			LAB		
	MDS	SDP	TRI	MDS	SDP	TRI
A0 / m	0.08	0.17	0.14	0.44	0.45	0.33
A2 / m	0.07	0.14	0.13	0.14	0.22	0.23
Δ / m	0.01	0.03	0.01	0.30	0.23	0.10

VI. EXPERIMENTAL RESULTS

The following sections present the experimental results. First, the improvement of the anchors' APE, using an additional CU with two CMs, for both scenarios and two CU positions, is presented in Sections V-A and V-B. Finally, the results of the anchor calibration, by means of alignment with the CU, are presented with the use of four CMs on the CU for two positions in the LAB scenario in Section V-C.

A. Improving the APE With a Calibration Unit

A test on the real anchor network system was performed to test anchor's network system, validate simulation results, confirm the use of simulations for determining the optimal CU position, and validate the anchor calibration method. Due to the number of anchors used in the GYM scenario, the test used A2 configuration and positions, obtained using prior simulations.

In the GYM scenario, the APE improved by 0.01 m with the MDS, 0.03 m with the SDP, and 0.01 m with the TRI method (see Table V). In the LAB scenario, the APE improved by 0.30 m with the MDS, 0.23 m with the SDP, and 0.10 m with the TRI method. In both scenarios, the MDS method had the lowest APE for the A0 and A2 configurations. The SDP and TRI methods had similar APE values for the A2 configuration in both scenarios, with a difference of 0.01 m. The MDS method gave results with the APE that were two times smaller in the GYM and 1.5 times smaller in the LAB scenario compared with the SDP and TRI methods.

The average APEs were calculated from 40 measurement sets for the xyz , xy , x , y , and z coordinates for all three localization methods, the GYM scenario (see Fig. 9), and the LAB scenario (see Fig. 10). The APE was smaller with the CU deployed regardless of the localization method used (all the blue marks are under the red marks).

In the GYM scenario, the STDs of the APEs were below 0.01 m for APE and $APE(z)$ and below 0.002 m for $APE(xy)$, $APE(x)$, and $APE(y)$ for the A0 and A2 configurations and all three localization methods.

In the LAB scenario, the STDs of the APEs were different for the A0 and A2 configurations and all three localization methods. The STDs of the APE and $APE(z)$ for the A0 configuration were below 0.05 m for the MDS, 0.06 m for the SDP, and 0.03 m for the TRI method (see Fig. 10, red marks). The STDs of the APE and $APE(z)$ for the A2 configuration were 0.02 m for the MDS, 0.03 m for the SDP, and 0.04 for the TRI method (see Fig. 10, blue marks). The STDs of $APE(xy)$, $APE(x)$, and $APE(y)$ were below 0.01 m for all the localization methods and both configurations.

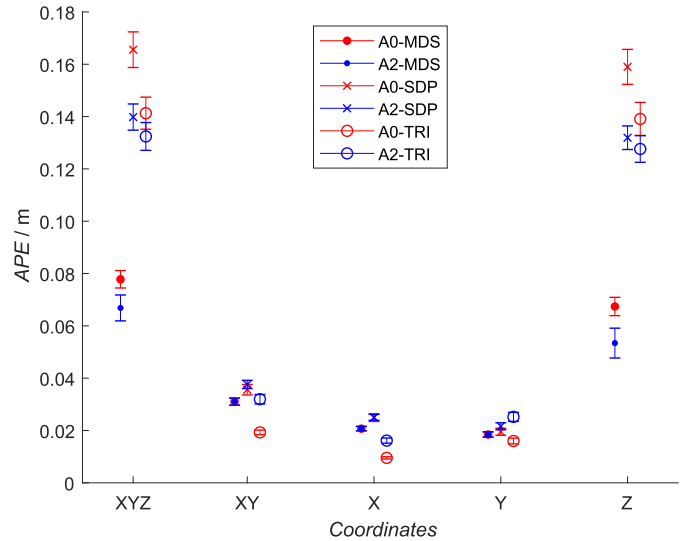


Fig. 9. Mean APE values computed from 40 measurement sets for all the localization methods and A0 and A2 configurations with the STD for the GYM scenario. Results are displayed as a function of the coordinates xyz , yx , x , y , and z used for the APE calculation.

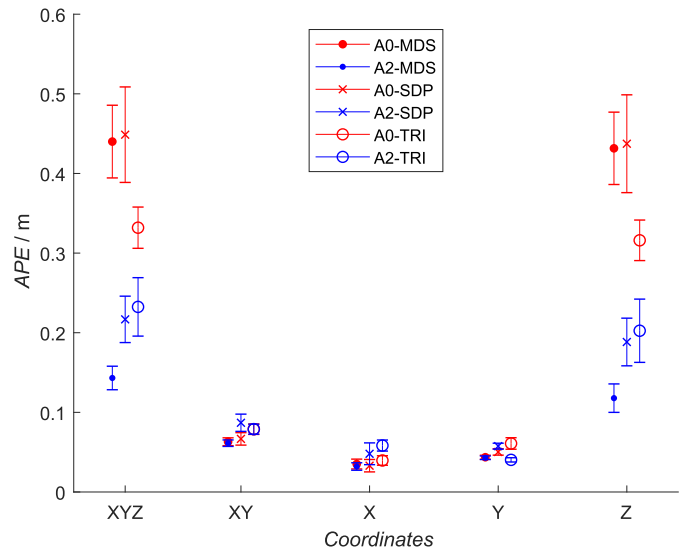


Fig. 10. Mean APE values computed from 40 measurement sets for all the localization methods and A0 and A2 configurations with the STD for the LAB scenario. Results are displayed as a function of the coordinates xyz , yx , x , y , and z used for the APE calculation.

The difference between APE and $APE(z)$ in the GYM scenario was smaller than 0.01 m for the MDS and the SDP methods and smaller than 0.005 m for the TRI method for the A0 and A2 configurations. The difference between the APE and $APE(z)$ in the LAB scenario was 0.01 m with the MDS and the SDP methods and smaller than 0.005 m with the TRI method for the A0 configuration. However, for the A2 configuration, the differences between APE and $APE(z)$ were 0.03 m with all three methods. For further analysis of $APE(xy)$, $APE(x)$, $APE(y)$, and $APE(z)$ from the data in Figs. 9 and 10 were normalized with the APE. In this case, $APE(z)$ represents over 90% of the APE, and $APE(xy)$, $APE(x)$, and $APE(y)$ represent, on average, 21% of the APE.

TABLE VI

EXPERIMENTAL APE FOR THE SECOND POSITION OF CU FOR ANCHOR LOCALIZATION WHEN A0 AND A2 IS USED FOR BOTH SCENARIOS

	GYM			LAB		
	MDS	SDP	TRI	MDS	SDP	TRI
A0 / m	0.08	0.16	0.14	0.41	0.41	0.32
A2 / m	0.07	0.14	0.12	0.16	0.21	0.25
Δ / m	0.01	0.02	0.02	0.25	0.20	0.07

TABLE VII

MEAN ERROR AND STD FOR THE MEASURED DISTANCES FOR THE GYM AND LAB SCENARIO IN THE OPTIMAL POSITION (P1)

	GYM	LAB
Bias / m	0.06	0.10
Std / m	0.05	0.13

B. Nonoptimal Position of the Calibration Unit

To confirm the APE improvement utilizing the CU, additional measurements with the CU in different positions were made. The CU was moved from the nonoptimal position P2 to the optimal position P1 for both scenarios presented in Figs. 4 and 5.

In the GYM scenario, the APE decreased by 0.01 m with the MDS, 0.02 m with the SDP, and with the TRI method when implementing the A2 instead of the A0 configuration (see Table VI). In the LAB scenario, the APE decreased by 0.25 m with the MDS, 0.20 m with the SDP, and 0.07 m with the TRI method.

A comparison of the values from Tables V and VI for the LAB scenario shows smaller APE improvements when the CU was used in the nonoptimal position compared with the optimal one. On average, the improvement in the nonoptimal position was more than 0.03 m less than in the optimal position for all the localization methods in the LAB scenario. In the GYM scenario, the APE values for the A2 configuration are the same. The only exception was with the TRI method, which had a 0.01 m larger APE in the nonoptimal position. The APE values were almost two times higher in NLOS conditions (LAB) than in LOS conditions (GYM).

The mean-bias error of the measured distances and the mean STD, calculated from 40 measurement sets, are presented in Table VII. The NLOS conditions in the LAB scenario gave an almost two-times-higher mean error and a more than two-times-higher STD, in comparison to the LOS conditions in the GYM scenario.

C. Anchor Calibration in the Working Coordinate System

To assess the presented anchor-calibration method with the CU, a test of the anchor localization in the working coordinate system was conducted. It used four CMs on the CU in the LAB scenario, with the CU in two positions, i.e., optimal and nonoptimal, as presented as P1 and P2 in Figs. 4 and 5.

In the optimal position P1, the APE values were smaller compared with the nonoptimal position P2. They decreased by 0.12, 0.04, and 0.34 m with the MDS, SDP, and TRI methods (see Table VIII).

TABLE VIII

ANCHOR-CALIBRATION RESULTS, ALIGNMENT WITH KNOWN CALIBRATION-MODULE POSITIONS

		MDS	SDP	TRI
P1	A4 / m	0.32	0.36	1.06
P2	A4 / m	0.44	0.40	1.40

VII. DISCUSSION

Previous work introduced the use of a CU as a feature to interconnect multiple anchors. This is beneficial if the anchors do not have a ranging capability due to obstacles or out-of-range distances between the anchors. This article presents an anchor-calibration method that uses additional CMs to improve the anchor localization and also localize the anchors in a working coordinate system. First, it was shown through simulations that the anchor-calibration accuracy can be improved by adding a feature, such as a CU. Second, the simulation results were validated with an experiment on a real system in 3-D. Finally, an anchor calibration in a working coordinate system in 3-D was performed and evaluated.

The simulation results showed a decrease of the APE for both scenarios and all the localization methods when additional CMs were used (see Table III). When comparing the APE improvement as an absolute value per added CM, the A1 configuration had the best results. compared with the best A16 configuration, and the values were over seven times lower with the MDS method and over 12 times lower when using the SDP and TRI methods. Even though the APE decreased further with more CMs used, the growing number of CMs raises the overall price and complexity of the system. It is worth noting that the APE improvement did not change linearly but decreased exponentially when the number of newly added CMs is increased. Therefore, the optimal number of CMs used should be determined by the permissible APE value and the available resources. Simple square-shape simulation configurations were chosen so that they could be easily replicated for the experiment.

Another parameter that could possibly improve the accuracy of the anchor coordinates is the height difference between the anchor and the CM. The height of the anchor placement was limited in the real-life experiments; however, it was possible to avoid and overcome those limitations through simulations. The height difference was increased to the height that corresponded to the length of the edges of the anchor's floor layout. These outer boundaries on the floor, described by the positions of the anchors, are shown in Figs. 4 and 5 and Table I. The simulation results showed that increasing the height difference between the anchors and the CM reduced the values of the APE (see Table IV). This reduction was seen up to the point where the height difference was equal to the length of one-half of the anchor's floor-layout edge.

The experiments in the GYM and LAB confirmed that the APE could be reduced by including the CU in the measurement. In the GYM scenario, the APE values decreased by at least 0.01 m and in the LAB by 0.07 m, with the TRI method, to 0.30 m, with the MDS method (see Tables V and VI). Simulation results predicted a greater reduction of the APE for

the LAB scenario, which the experimental results confirmed (see Table III). Of course, the simulation and experimental APE values differ; the main reasons could be that the simulations used a noise model without any bias. Those differences could be reduced in subsequent research by implementing a model that includes a nonlinear bias error of the distance measurements, the NLOS conditions, and the dependence of the measured distance on the anchors' orientations. The APE reductions with the SDP method were not directly compared due to the problems (see next paragraph) with the A0 configuration simulations. Those problems resulted in poor localization and, consequently, the simulation data gave much larger APE values than the experimental data.

When comparing the simulated and experimental results for the A2 configuration, obtained with the MSD and SDP methods, differences in the performance arose. In simulations, the SDP had smaller APE values than the MDS method. However, the experiments yielded contrasting results. As mentioned earlier, the SDP method proved to be noise sensitive. In additional simulations, the distances included the bias error. If there was no additional bias error present, the SDP method gave better results. However, its performance reduced faster compared with the MDS method when the mean-bias error increased. For the values of the mean-bias error present in the experiments, the MDS method outperformed the SDP method.

A comparison of the errors for all the coordinate combinations showed that the largest contribution to the APE came from the error along the z -axis (see Figs. 9 and 10). When the CU was utilized, the APE decreased, with the largest change being on the z -axis. Small STD values of the mean APE value in the GYM scenario indicate that our anchor system and the presented anchor-calibration procedure are stable. In the LAB scenario, with the NLOS and time-varying conditions, larger STD values were present. NLOS conditions in LAB scenario, along with setup configuration, resulted in larger APE values (see Tables V and VI). In the GYM scenario with LOS conditions and, therefore, smaller bias error and STD in distance measurements (see Table VII), a smaller number of measurement sets can be used for anchor calibration. The number of measurement sets should be increased for more severe NLOS conditions, as in the LAB scenario, within time constraints. With a bigger number of measurement sets, rather than measured distances in each set, different conditions are recorded for all anchor pairs.

The results obtained for the LAB scenario (see Tables V and VI) confirmed that the optimal position can be attained through simulations, where the APE improvement is smaller in the nonoptimal position. Therefore, the simulations are a suitable tool to evaluate the optimal position in both simple and more complex environments. Results from the GYM scenario did not provide the APE difference between different positions due to the relatively small position change of CU in a bigger anchor layout. Due to the complexity associated with anchor configuration, it is difficult to generalize the CU setup options. Experimental results have shown that a larger height difference between the anchors and the CU, and between the anchors themselves, gives better localization results. However, both parameters

TABLE IX
AVERAGE 2-D POSITIONAL ERROR FOR ANCHOR CALIBRATION IN PREVIOUS RESEARCH AND THIS ARTICLE

	no. anchors (no. CM)	2D / m	3D / m
Nakamura <i>et al.</i> [21]	8 (0)	0.95	/
Müller <i>et al.</i> [23]	4 (1)	1.20	/
Van de V. <i>et al.</i> [24]	4 (1)	0.08	/
Scenario GYM	16 (2)	0.03	0.07
Scenario LAB	12 (2)	0.06	0.14

are usually limited by the realistic environment where the RTLS will operate. The APE results of both scenarios and both positions showed that the MDS localization method is the most suitable for our anchor-calibration method.

The results of the anchor calibration from previous research and from this article are compared in Table IX. All the presented error values are associated with aligning the localized anchors with their reference positions in 2-D. Through this, the performance of anchor-calibration methods can be evaluated even though the anchors are not placed in a coordinate system where the RTLS could operate. The results are comparable with the first part of this article, where the effects of the CU on the anchor calibration were studied. When comparing the results within Table IX, parameters such as the anchor configuration and the number of anchors have to be taken into consideration. The APE values show the good performance of the presented calibration method, in simple LOS as well as in NLOS conditions, and complex, more realistic environments.

The presented anchor calibration method is a useful tool for RTLS initialization without external measurement equipment. In cases with hybrid systems [5], it would be beneficial as calibration of the UWB system also calibrates primary systems where RTLS uses smaller anchor systems method enables fast reconfigurability [6]. In industrial environments, the calibration method provides possibilities of merging coordinate systems of different RTLS based on different technologies and covering different areas [7], [8].

Finally, the proposed anchor-calibration method was tested in a real experiment, where the setup of 12 anchors and four CMs on the CU, in the desired working coordinate system, was placed. In this way, the alignment of the localized anchor to the work coordinate system was possible. With the MDS method, an anchor calibration with a 3-D error of 0.32 m was achieved.

VIII. CONCLUSION

This article presents a novel approach to a self-localizing anchor-system calibration that uses a CU for improved localization accuracy. This study confirmed that the use of the CU decreases the average positional error of the anchors in 3-D localization systems. In addition, the simulations were confirmed to be a valid tool for determining the best position of the CU. Finally, the first demonstration of an anchor calibration with a CU and anchors localized in the working coordinate system in 3-D was presented. It had an error of 0.32 m.

The performance of the three different localization methods was tested, and the results showed that the MDS method had the best localization accuracy. Using a CU enables all the applications to improve anchor-localization accuracy. The potential downside of using a CU for the anchor calibration is the need to use additional modules, affecting the complexity and the price of the localization system.

In future work, an analysis of the effects of adding a CU to anchor configurations, where a complete EDM cannot be assembled from mere measurements, would be beneficial. For the EDM completion, additional steps in the localization algorithms should be taken. This would enable the localization of all the anchors in the RTLS, and consequently, the anchor calibration could be used universally for almost all RTLS applications and their specific environmental requirements.

ACKNOWLEDGMENT

The authors would like to thank Assist. Prof. G. Štebe, M.S., from the Faculty of Civil and Geodetic Engineering for the reference-point measurements and B. Jakopin for his valuable comments during the preparation of this article.

REFERENCES

- [1] K. Guo *et al.*, "Ultra-wideband-based localization for quadcopter navigation," *Unmanned Syst.*, vol. 4, no. 1, pp. 23–34, Jan. 2016.
- [2] X. Tang and S. Mandal, "Indoor occupancy awareness and localization using passive electric field sensing," *IEEE Trans. Instrum. Meas.*, vol. 68, no. 11, pp. 4535–4549, Nov. 2019.
- [3] A. R. J. Ruiz and F. S. Granja, "Comparing ubisense, BeSpoon, and DecaWave UWB location systems: Indoor performance analysis," *IEEE Trans. Instrum. Meas.*, vol. 66, no. 8, pp. 2106–2117, Aug. 2017.
- [4] S. He and X. Dong, "High-accuracy localization platform using asynchronous time difference of arrival technology," *IEEE Trans. Instrum. Meas.*, vol. 66, no. 7, pp. 1728–1742, Jul. 2017.
- [5] M. Kolakowski, "A hybrid BLE/UWB localization technique with automatic radio map creation," in *Proc. 13th Eur. Conf. Antennas Propag. (EuCAP)*, Krakow, Poland, Jun. 2019, pp. 1–4.
- [6] J. Wang, Y. Tang, J.-M. Muñoz-Ferreras, R. Gómez-García, and C. Li, "An improved indoor localization solution using a hybrid UWB-Doppler system with Kalman filter," in *Proc. IEEE Radio Wireless Symp. (RWS)*, Anaheim, CA, USA, Jan. 2018, pp. 181–183.
- [7] A. Martinelli, S. Jayousi, S. Caputo, and L. Mucchi, "UWB positioning for industrial applications: The galvanic plating case study," in *Proc. Int. Conf. Indoor Positioning Indoor Navigat. (IPIN)*, Pisa, Italy, Sep. 2019, pp. 1–7.
- [8] W. Wang, Z. Zeng, W. Ding, H. Yu, and H. Rose, "Concept and validation of a large-scale human-machine safety system based on real-time UWB indoor localization," in *Proc. IEEE/RSJ Int. Conf. Intell. Robots Syst. (IROS)*, Macau, China, Nov. 2019, pp. 201–207.
- [9] C. Zhou, T. Xu, and H. Dong, "Distributed locating algorithm MDS-MAP (LF) based on low-frequency signal," *Comput. Sci. Inf. Syst.*, vol. 12, no. 4, pp. 1289–1305, Nov. 2015.
- [10] W. Cui, C. Wu, W. Meng, B. Li, Y. Zhang, and L. Xie, "Dynamic multidimensional scaling algorithm for 3-D mobile localization," *IEEE Trans. Instrum. Meas.*, vol. 65, no. 12, pp. 2853–2865, Dec. 2016.
- [11] Y. Shang, W. Rumi, Y. Zhang, and M. Fromherz, "Localization from connectivity in sensor networks," *IEEE Trans. Parallel Distrib. Syst.*, vol. 15, no. 11, pp. 961–974, Nov. 2004.
- [12] N. Krislock and H. Wolkowicz, "Explicit sensor network localization using semidefinite representations and facial reductions," *SIAM J. Optim.*, vol. 20, no. 5, pp. 2679–2708, Jan. 2010.
- [13] D. Drusvyatskiy, N. Krislock, Y.-L. Voronin, and H. Wolkowicz, "Noisy Euclidean distance realization: Robust facial reduction and the Pareto frontier," *SIAM J. Optim.*, vol. 27, no. 4, pp. 2301–2331, Jan. 2017.
- [14] D. K. Goldenberg *et al.*, "Localization in sparse networks using sweeps," in *Proc. 12th Annu. Int. Conf. Mobile Comput. Netw. (MobiCom)*, Los Angeles, CA, USA, Sep. 2006, pp. 110–121.
- [15] N. B. Priyantha, H. Balakrishnan, E. Demaine, and S. Teller, "Anchor-free distributed localization in sensor networks," in *Proc. 1st Int. Conf. Embedded Netw. Sensor Syst.*, Los Angeles, CA, USA, Nov. 2003, pp. 340–341.
- [16] A. Savvides, C.-C. Han, and M. B. Strivastava, "Dynamic fine-grained localization in ad-hoc networks of sensors," in *Proc. 7th Annu. Int. Conf. Mobile Comput. Netw. (MobiCom)*, Rome, Italy, Jul. 2001, pp. 166–179.
- [17] Y. Kuang, S. Burgess, A. Torstensson, and K. Åström, "A complete characterization and solution to the microphone position self-calibration problem," in *Proc. IEEE Int. Conf. Acoust., Speech Signal Process.*, Vancouver, BC, Canada, May 2013, pp. 3875–3879.
- [18] K. Batstone, M. Oskarsson, and K. Åström, "Towards real-time time-of-arrival self-calibration using ultra-wideband anchors," in *Proc. Int. Conf. Indoor Positioning Indoor Navigat. (IPIN)*, Sapporo, Japan, Sep. 2017, pp. 1–8.
- [19] Y. Zhou, C. L. Law, and F. Chin, "Construction of local anchor map for indoor position measurement system," *IEEE Trans. Instrum. Meas.*, vol. 59, no. 7, pp. 1986–1988, Jul. 2010.
- [20] P. Duff and H. Muller, "Autocalibration algorithm for ultrasonic location systems," in *Proc. 7th IEEE Int. Symp. Wearable Comput.*, White Plains, NY, USA, vol. 3, Oct. 2003, p. 62.
- [21] K. Nakamura and K. Sakamura, "Sub-meter accuracy localization system using self-localized portable UWB anchor nodes," in *Proc. 1st IEEE Global Conf. Consum. Electron.*, Tokyo, Japan, Oct. 2012, pp. 695–698.
- [22] D. Moore, J. Leonard, D. Rus, and S. Teller, "Robust distributed network localization with noisy range measurements," in *Proc. 2nd Int. Conf. Embedded Netw. Sensor Syst. (SenSys)*, Baltimore, MD, USA, Nov. 2004, pp. 50–61.
- [23] M. Müller, J. Lategahn, L. Telle, and C. Röhrig, "Automatic anchor calibration in IEEE 802.15. 4a networks," in *Proc. 8th Workshop Positioning, Navigat. Commun.*, Dresden, Germany, Apr. 2011, pp. 67–71.
- [24] S. Van De Velde, P. Van Torre, and H. Steendam, "Fast and robust anchor calibration in range-based wireless localization," in *Proc. 7th Int. Conf. Signal Process. Commun. Syst. (ICSPCS)*, Gold Coast, QL, Australia, Dec. 2013, pp. 1–6.
- [25] D. Neirynek, E. Luk, and M. McLaughlin, "An alternative double-sided two-way ranging method," in *Proc. 13th Workshop Positioning, Navigat. Commun. (WPNC)*, Bremen, Germany, Oct. 2016, pp. 1–4.
- [26] A. Cazzorla, G. De Angelis, A. Moschitta, M. Dionigi, F. Alimenti, and P. Carbone, "A 5.6-GHz UWB position measurement system," *IEEE Trans. Instrum. Meas.*, vol. 62, no. 3, pp. 675–683, Mar. 2013.
- [27] K. S. Arun, T. S. Huang, and S. D. Blostein, "Least-squares fitting of two 3-D point sets," *IEEE Trans. Pattern Anal. Mach. Intell.*, vol. PAMI-9, no. 5, pp. 698–700, Sep. 1987.
- [28] Y. Shang and W. Ruml, "Improved MDS-based localization," in *Proc. IEEE INFOCOM*, Hong Kong, vol. 4, Mar. 2004, pp. 2640–2651.
- [29] L. Vandenberghe and S. Boyd, "Semidefinite programming," *SIAM Rev.*, vol. 38, no. 1, pp. 49–95, Mar. 1996.
- [30] F. Santos, "Localization in wireless sensor networks," *ACM J.*, vol. 5, pp. 1–19, Nov. 2008.



Peter Krapež received the M.Sc. degree in electrical engineering from the Faculty of Electrical Engineering, University of Ljubljana, Ljubljana, Slovenia, in 2017, where he is currently pursuing the Ph.D. degree with the Laboratory of Robotics, Department of Measurement and Robotics, Faculty of Electrical Engineering.



Marko Munih (Member, IEEE) received the Ph.D. degree in electrical engineering from the Faculty of Electrical Engineering, University of Ljubljana (UL), Ljubljana, Slovenia.

From 2004 to 2006, he was the Head of the Department for Measurements and Process Control, Faculty of Electrical Engineering, UL, where he is currently a Full Professor and the Head of the Laboratory of Robotics.